Cell

Chemokine Guidance of Central Memory T Cells Is Critical for Antiviral Recall Responses in Lymph Nodes

Jung Hwan Sung,[1] Han Zhang,[1] E. Ashley Moseman,[1] David Alvarez,[1] Matteo Iannacone,[1] Sarah E. Henrickson,[1] Juan C. de la Torre,[2] Joanna R. Groom,[3] Andrew D. Luster,[3] and Ulrich H. von Andrian[1,*]
[1]Department of Microbiology and Immunobiology, Harvard Medical School, Boston, MA 02115, USA
[2]Department of Immunology and Microbial Science, The Scripps Research Institute, 10550 North Torrey Pines Road, La Jolla, CA 92037, USA
[3]Center for Immunology and Inflammatory Diseases, Division of Rheumatology, Allergy, and Immunology, Massachusetts General Hospital, Harvard Medical School, Charlestown, MA 02129, USA
*Correspondence: uva@hms.harvard.edu
http://dx.doi.org/10.1016/j.cell.2012.08.015

SUMMARY

A defining feature of vertebrate immunity is the acquisition of immunological memory, which confers enhanced protection against pathogens by mechanisms that are incompletely understood. Here, we compared responses by virus-specific naive T cells (T_N) and central memory T cells (T_{CM}) to viral antigen challenge in lymph nodes (LNs). In steady-state LNs, both T cell subsets localized in the deep T cell area and interacted similarly with antigen-presenting dendritic cells. However, upon entry of lymph-borne virus, only T_{CM} relocalized rapidly and efficiently toward the outermost LN regions in the medullary, interfollicular, and subcapsular areas where viral infection was initially confined. This rapid peripheralization was coordinated by a cascade of cytokines and chemokines, particularly ligands for T_{CM}-expressed CXCR3. Consequently, in vivo recall responses to viral infection by CXCR3-deficient T_{CM} were markedly compromised, indicating that early antigen detection afforded by intranodal chemokine guidance of T_{CM} is essential for efficient antiviral memory.

INTRODUCTION

A hallmark of the vertebrate immune system is its capacity to remember previous exposures to an infectious pathogen. This unique feature, called "immunological memory," is embodied in long-lived, self-renewing lymphocytes that possess the ability to respond more rapidly and vigorously to repeated exposure to antigens (Ags) than naive lymphocytes. Understanding the mechanisms by which immunological memory is exerted is of pivotal importance for the design of effective vaccines (Pulendran and Ahmed, 2006).

Numerous studies have demonstrated that memory T cells have intrinsic qualities that allow more rapid responses upon exposure to recall Ag, as compared to naive T cells (T_N) (Sprent and Surh, 2002). However, more recent in vivo studies suggest that such cell-intrinsic differences may not be the only mechanism to explain how memory T cells "remember" previous challenges. One case in point is effector memory T cells (T_{EM}), which are a subset of Ag-experienced T cells that are thought to arise from effector T cells (T_{Eff}) and retain many properties of T_{Eff} (Sallusto et al., 1999). Unlike T_N, which recirculate through lymph nodes (LNs) to search for their Ag, T_{EM} reside in nonlymphoid peripheral tissues (von Andrian and Mackay, 2000). The enhanced protection against reinfection afforded by T_{EM} can be explained, at least in part, by their privileged access to tissues that are particularly vulnerable to repeated invasions by pathogens (Gebhardt et al., 2009; Irla et al., 2010; Masopust et al., 2001).

Whereas tissue-resident T_{EM} provide the first line of defense against reinfection, central memory T cells (T_{CM}) participate in the continuous immune surveillance of LNs, similar to T_N. LNs play a crucial role in the initiation, amplification, and reactivation of immune responses to peripheral Ags (von Andrian and Mempel, 2003). They achieve this function by monitoring the lymph, which is generated in peripheral tissues by exudation of aqueous fluid from capillaries and drained to local LNs via afferent lymph vessels. This drainage system serves as an essential conduit through which free Ag, migratory Ag-carrying dendritic cells (DCs), and also intact microorganisms are transported to LNs for the initiation of adaptive immune responses.

While patrolling through lymphoid organs, resting T_{CM} exert limited immediate effector functions. However, upon Ag rechallenge, T_{CM} release interferon (IFN)γ and divide rapidly, giving rise to large numbers of T_{Eff} (Sallusto et al., 1999). Because invading viruses can proliferate exponentially in a defenseless host, the accelerated initiation of T_{Eff} activity afforded by T_{CM} reactivation is thought to provide a pivotal mechanism to curtail viral disease. However, the mechanisms that render LN-resident T_{CM} responses more expedient than those by T_N remains unclear. How does T cell memory manifest itself at the single-cell level?

We sought to address these questions by using intravital imaging strategies to compare the response kinetics of T_N and T_{CM} in virally infected LNs. First, we asked whether there are differences in the migratory or interactive behavior of T_{CM} and

T_N that might differentially affect their ability to contact Ag-bearing DCs in the deep LN cortex. Second, we tested the hypothesis that T_{CM} may have preferred access to intranodal recall Ag outside of the T cell area. This possibility was suggested by recent findings that lymph-borne viruses are rapidly captured by macrophages in the subcapsular sinus (SCS) and medulla of LNs (Junt et al., 2007; Iannacone et al., 2010; Moseman et al., 2012). We reasoned that, although macrophage capture of viruses is important to prevent systemic dissemination, the restricted distribution of early viral replication in the LNs may pose a challenge for T cells to rapidly find their cognate Ag.

Our results demonstrate that the response kinetics of T_{CM} and T_N to Ag-bearing DCs within the T cell area are surprisingly similar. By contrast, T_{CM} were more efficient at detecting and responding to viral Ag within the first few hours after Ag appearance in peripheral areas of LNs, which are poorly accessible to T_N. Our results elucidate how accelerated detection of Ag by T_{CM} is directed by a coordinated cascade of cytokines and chemokines, particularly ligands for CXCR3. When directed migration of T_{CM} was disrupted, T_{CM} reactivation was delayed and viral clearance was compromised, indicating that antiviral recall responses are critically dependent on this chemokine pathway to enable viral Ag detection by $CD8^+$ memory cells.

RESULTS

T_N versus T_{CM} Responses to Ag-Presenting DCs in Deep LN Cortex

Upon peripheral infection, tissue DCs carry pathogen-derived Ag into the deep T-cell-rich cortex of draining LNs (Alvarez et al., 2008). $CD8^+$ T_N that access LNs via high endothelial venules (HEV) become activated when they come upon a DC presenting cognate Ag. This process involves three sequential phases that are associated with distinct phenotypic and functional changes in T_N (Henrickson and von Andrian, 2007; Mempel et al., 2004; Miller et al., 2004). Initially, T_N engage in brief serial contacts with multiple DCs and upregulate activation markers (phase 1). After a few hours, they form prolonged stable conjugates that persist for several hours and lead to secretion of effector cytokines (phase 2). On the second day, T cells regain their mobility and proliferate (phase 3). It has been unclear whether T_{CM} display similar dynamics in LNs.

To address this question, we compared the kinetics of $CD8^+$ T_{CM} and T_N proliferation, effector differentiation, and interactive behavior in popliteal LNs (popLNs) upon encounter of Ag-presenting DCs (Figure S1A available online). Briefly, T_N were harvested from T cell receptor (TCR) transgenic P14 mice, which recognize an immunodominant peptide from lymphocytic choriomeningitis virus (LCMV) glycoprotein (Pircher et al., 1989). Some P14 T_N were activated in vitro and were cultured for $\geq$9 days in recombinant IL-15 to generate T_{CM}-like cells as described (Manjunath et al., 2001). Recipient mice were injected subcutaneously (s.c.) into a footpad with Ag-pulsed DCs. The recipients were injected intravenously (i.v.) 18 hr later with P14 T_N or T_{CM}, and intranodal T cell activation and proliferation were monitored.

Upon encounter of Ag-pulsed DCs, CD69, a marker of early T cell activation, was upregulated by T_N and T_{CM} with similar kinetics (Figure 1A), and both subsets began to proliferate (Figure 1B). There was also no difference between T_N and T_{CM} in the rate of Ag-driven proliferation, which was estimated as the proliferative response to Ag-pulsed DCs minus the Ag-independent background proliferation of each subset (Figure 1C). Both T cell populations secreted IFNγ, but the response of T_{CM} was greater than that of T_N (Figure 1D).

Migratory and Interactive Behavior of T_N and T_{CM} in Deep LN Cortex

Having determined that the dynamics of T_{CM} and T_N responses to Ag-pulsed DCs were similar in most aspects, we next asked whether there were differences in migratory or interactive behavior. The microanatomic distribution of homed T_{CM} and T_N at steady state was similar, and >80% of cells localized to the deep T cell area (Figures 1E, 1F, and S1C). Using multiphoton intravital microscopy (MP-IVM) (Mempel et al., 2004), we observed that both T cell populations displayed similarly high motility in the deep cortex (Figure S1E).

Next, we compared the interaction dynamics of T_{CM} and T_N with Ag-presenting DCs (Figure S1A) (Henrickson et al., 2008). The duration of contacts with DCs was essentially the same for T_{CM} and T_N during the first 10 hr after adoptive T cell transfer (Figures 1G and S1D). DCs pulsed with a high peptide dose (10 μM) supported the formation of stable contacts with both T cell subsets within 2 to 4 hr after transfer (Figure 1G and Movie S1), resulting in equivalent reduction in their migratory velocity (Figure S1E). T_{CM} and T_N also interacted similarly with DCs pulsed with 100 pM peptide concentration, which represented the lowest pulsing dose that allowed DCs to induce full-fledged proliferation of T_{CM} and T_N (Figure S1D). Neither T_{CM} nor T_N displayed prolonged interactions with DCs pulsed with 10 pM peptide, which was below the threshold that triggered proliferation of either subset. We conclude that the intranodal motility and interaction kinetics of T_N and T_{CM} with Ag-pulsed DCs are roughly equivalent in character and magnitude. Moreover, the interactive behavior of T_{CM} depends upon the dose of cognate Ag presented by DCs, which is consistent with previous findings with T_N (Henrickson et al., 2008).

Response Kinetics of T_N and T_{CM} upon LCMV Infection in LNs

In light of these MP-IVM observations, we wondered whether T_{CM} are distinguishable from T_N by other features that enable rapid recall responses without requiring migratory DCs from the periphery. This seemed appealing because viruses in the interstitium can access local lymph vessels and accumulate in draining LNs within minutes after deposition under the skin (Junt et al., 2007). By contrast, peripheral DCs require many hours to several days to reach LNs (Alvarez et al., 2008). Because some viruses proliferate rapidly in host LNs, T_{CM} could not provide meaningful protection if their function depended upon initial encounters with migratory DCs.

Indeed, when footpads of mice were injected s.c. with infectious LCMV, approximately half of virus-specific T_{CM} upregulated CD69 within 8 hr, whereas CD69 expression on T_N lagged behind (Figure 1H). The onset of Ag-driven T_{CM} proliferation was also accelerated (Figures 1I and 1J). Thus, the early kinetics of CD69 induction and proliferation were significantly faster for

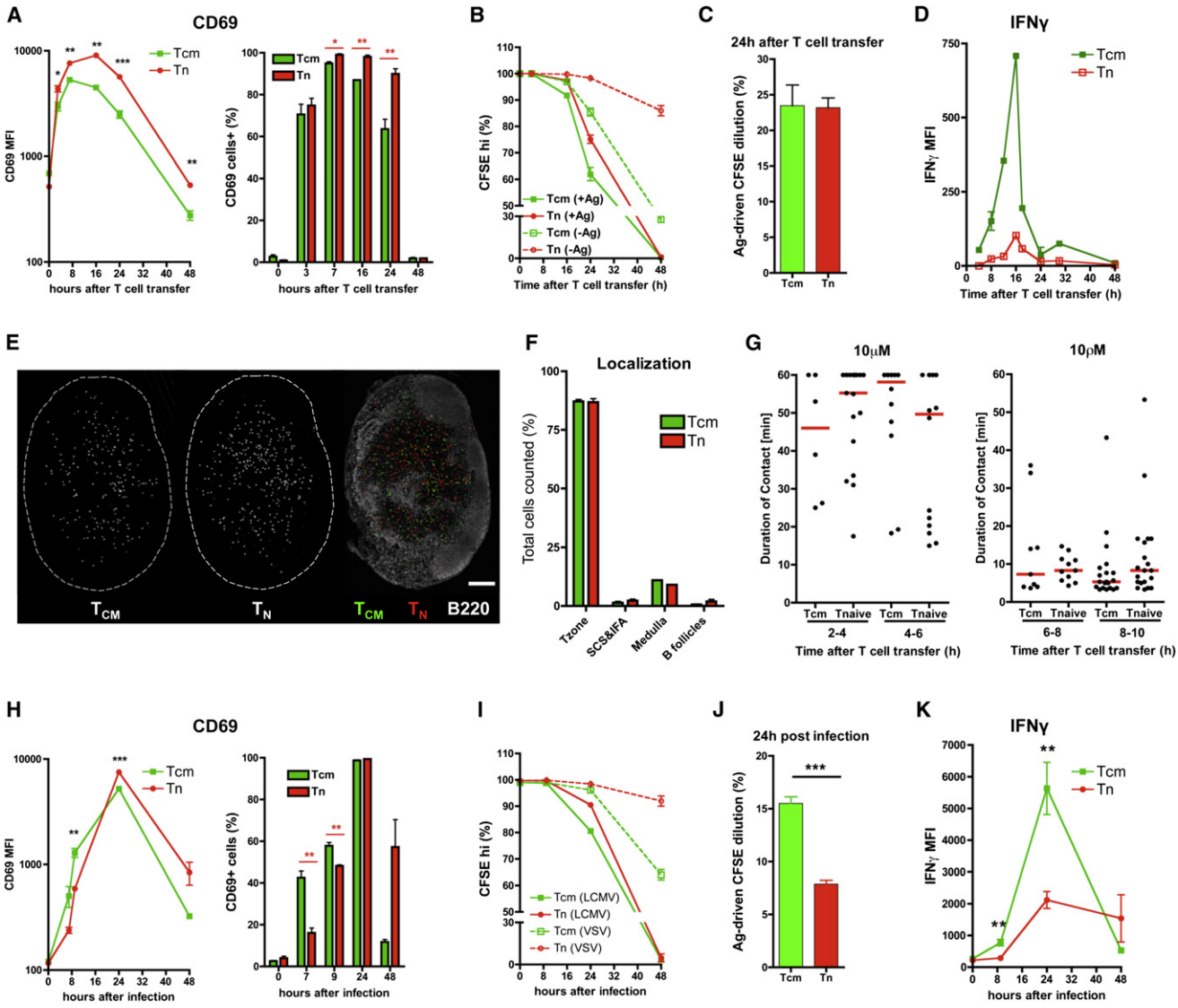

Figure 1. Kinetics of T_N and T_{CM} Responses to Ag-Presenting DCs and LCMV Infection

(A–D) Kinetics of T_N and T_{CM} activation upon encounter of Ag-pulsed DCs in deep LN cortex. (A) Induction of CD69 measured as mean fluorescence intensity (MFI; left) and percent positive cells (right). (B) Proliferation, assessed by CFSE dilution ($CFSE^{hi}$ represent undivided cells). (C) Ag-driven proliferation, calculated as the difference in percentage of divided P14 cells after encounter of DCs pulsed with cognate versus control Ag. (D) IFNγ secretion.

(E) Micrographs showing the distribution of adoptively transferred T_{CM} and T_N in popLNs at steady state. Scale bar, 150 μm.

(F) Percentage of T_{CM} and T_N within indicated LN compartments at steady state (n = 3).

(G) MP-IVM analysis of T_{CM} and T_N interactions with DCs pulsed with 10 μM or 10 ρM of peptide Ag.

(H–K) Kinetics of T_N and T_{CM} activation upon s.c. LCMV infection into a footpad. (H) Induction of CD69. (I) Proliferation, assessed by CFSE dilution ($CFSE^{hi}$ represent undivided cells). (J) Ag-driven proliferation, calculated as the difference in percentage of divided P14 cells after LCMV (cognate) versus VSV (control) infection. (K) IFNγ secretion.

**p < 0.01 and ***p < 0.001. Error bars represent mean ±SEM. See also Figure S1 and Movies S1 and S2.

T_{CM} than T_N upon viral infection in LNs, whereas both subsets responded equally when T cells homed to uninfected LNs that contained Ag-pulsed DCs. By contrast, T_{CM} mounted a more vigorous IFNγ response in both settings (Figures 1D and 1K).

Visualization of LCMV Replication in LNs

Given the faster early response kinetics of T_{CM} versus T_N upon challenge with live virus, but not with Ag-pulsed DCs, we asked whether this disparity was due to differential accessibility of viral Ag to the two T cell subsets. Thus, mice were infected in a footpad with LCMV-enhanced green fluorescent protein (LCMV-EGFP), which drives green fluorescent protein (GFP) expression in infected cells (Emonet et al., 2009). At 8 hr after infection, GFP expression was detected in the SCS and in the medulla, but not in the T cell area of the popLN (Figures 2A and 2B). This peripheral localization of GFP reflected LCMV replication because

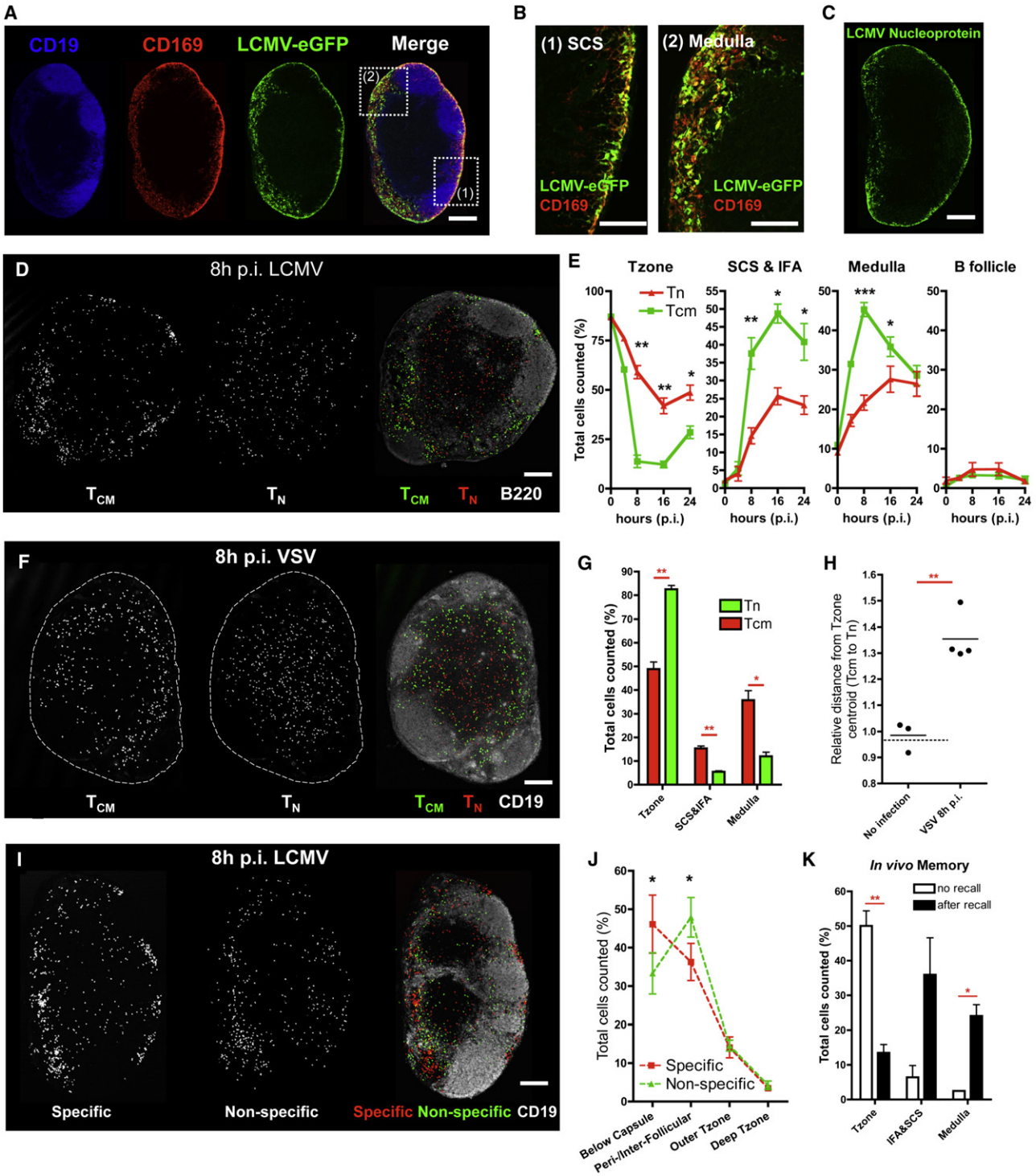

Figure 2. Differential Redistribution of T_N versus T_{CM} in Virally Infected LNs

(A–C) Micrographs of popLN sections 8 hr after footpad infection with LCMV-EGFP stained for leukocyte markers or viral Ags as indicated.

(D) Micrographs showing the distribution of adoptively transferred T_{CM} and T_N.

(E) Percentage of P14 T_{CM} and T_N within indicated LN compartments. n = 3–4.

(F) Micrographs showing the distribution of adoptively transferred P14 T_{CM} and T_N in popLNs 8 hr after footpad infection with VSV.

(G) Percentage of T_{CM} and T_N within indicated LN compartments. n = 3–4.

(H) Relative distance of T_{CM} and T_N from the centroid of the T cell area (calculated as the ratio of the median distances of T_{CM} to the median distance of T_N from centroid in each section).

staining of LCMV nucleoprotein gave an identical staining pattern (Figure 2C). GFP$^+$ viral host cells were predominantly macrophages, which included both the CD169^{hi} subset in the SCS and the CD169^{dim} subset in the medulla (Figure 2B).

Differential Redistribution of T_N versus T_{CM} in Virally Infected LNs

Having observed that early LCMV replication in LNs is restricted to peripheral macrophage-rich compartments, we adoptively transferred fluorescently tagged P14 T_{CM} and T_N to determine their intranodal distribution before and after LCMV infection. Whereas T_{CM} and T_N were both restricted to the deep T cell area at steady state, 8 hr after LCMV infection, ~90% of T_{CM} had relocalized to the medulla, interfollicular area (IFA), and SCS (Figures 2D, 2E, and S1C). T_N also peripheralized to some extent, which is consistent with recent observations in vaccinia-virus-infected LNs (Hickman et al., 2008). However, compared to T_{CM}, the kinetics and efficiency of T_N redistribution were substantially delayed and reduced, respectively (Figure 2E). These findings are in line with the idea that T_{CM}, by migrating preferentially toward infected host cells outside of the T cell area, may gain more rapid access to lymph-derived viral Ag than T_N.

T_{CM} Interact with Virally Infected Cells after Relocalization

Having established that T_{CM} redistribute rapidly upon viral challenge, we asked whether T_{CM} interact with infected APCs in their environment. Indeed, upon infection with LCMV-EGFP, many T_{CM} that had migrated to the SCS contacted GFP$^+$ CD169$^+$ SCS macrophages (Figure S2A). Interestingly, there was also a striking redistribution of CD11c$^+$ cells, which, in noninfected LNs, display a fairly uniform distribution throughout the organ (except for B follicles); by 8 hr after LCMV infection, CD11c$^+$ cells had formed dense clusters in the IFA and medulla (Figure S2B). Most CD11c^{bright} cells in these regions were GFP$^-$, yet many formed clusters with T_{CM} (Figure S2C). These cells likely represented DCs that cross-presented viral Ag acquired from infected macrophages. By 24 hr after infection, the peripheral CD11c$^+$ clusters had dissipated. Instead, CD11c staining was enhanced in the deep T cell area (Figure S2B), suggesting that the DCs migrated from the periphery to the deep cortex. Thus, following virus-induced peripheralization, T_{CM} appear poised to interact with both macrophages and DCs capable of presenting viral Ag.

Role of TCR Specificity

To address whether TCR specificity is relevant in the process of T_{CM} peripheralization, we assessed the redistribution of LCMV-specific T_{CM} and T_N upon infection with vesicular stomatitis virus (VSV), which is not antigenic for P14 cells. Even in this setting, T_{CM} peripheralized rapidly, whereas T_N remained mainly in the deep cortex (Figures 2F–2H), indicating that T_{CM} redistribute without requiring TCR stimulation. However, Ag specificity also played a role; in LCMV-infected LNs containing both specific (P14) and nonspecific (OT-I) T_{CM}, both subsets vacated the T cell area, but many P14 T_{CM} were tightly clustered in the outermost periphery, whereas nonspecific T_{CM} congregated in less superficial regions (Figures 2I and 2J). Moreover, MP-IVM imaging of T_{CM} in the superficial cortex of LCMV-EGFP-infected LNs showed that the nonspecific T_{CM} migrated more rapidly than virus-specific T_{CM}, which frequently arrested in vicinity to GFP$^+$ cells (Figures S2D–S2G and Movie S3). This suggests that specific and nonspecific T_{CM} may initially follow guidance cues that do not attract T_N, but subsequent encounter of cognate Ag allows T_{CM} to accumulate in immediate proximity to infected APCs.

Redistribution of In-Vivo-Generated T_{CM}

Although our in vitro method to generate T_{CM}-like CD8$^+$ T cells has been validated in multiple settings (Halin et al., 2005), it was important to assess whether our observations with adoptively transferred ex-vivo-differentiated Ag-experienced T cells reflected the behavior of endogenous T_{CM}. To address this, a small number of CD45.1$^+$ P14 T_N were injected into CD45.2$^+$ recipients that were then infected with LCMV. After 4 weeks, the distribution of CD45.1$^+$ memory cells in LNs was assessed before and after rechallenge with LCMV. At steady state, the largest fraction of CD45.1$^+$ memory cells was found in the T cell zone, whereas at 8 hr after rechallenge, the virus-specific T_{CM} had shifted into the IFA and medulla (Figures 2K and S2H–S2J). Thus, in-vivo-generated bona fide T_{CM} relocalize within LNs as rapidly as ex-vivo-differentiated T_{CM}-like cells.

CXCR3 Promotes T_{CM} Redistribution in LNs

Next, we sought to identify the molecular guidance cues for T_{CM} peripheralization. Interstitial lymphocyte migration is chiefly regulated by chemokines (Rot and von Andrian, 2004). Several chemokine receptors are upregulated on T_{CM} (Kaech et al., 2002), including CXCR3, which recognizes two ligands in C57BL/6 mice, CXCL9 and CXCL10. Indeed, both in-vivo- and in-vitro-generated T_{CM} were uniformly CXCR3$^+$, whereas T_N were CXCR3$^{low/-}$ (Figures 3A and S3A). Interestingly, expression of CXCR3 on T_{CM} in LCMV-draining LNs was 4.3-fold lower than on T_{CM} in contralateral LNs (Figure 3A), suggesting that the receptor was downmodulated due to ligand stimulation. This prompted us to compare the LCMV-induced relocalization of P14 T_{CM} and P14 CXCR3-KO T_{CM} in LNs. Prior to infection, both T_{CM} subsets were concentrated in the deep T cell area. However, 8 hr after infection, their distribution was strikingly different; P14 CXCR3-KO T_{CM} remained restricted to the deep cortex, whereas P14 T_{CM} accumulated in the medulla, SCS, and IFA (Figures 3B and 3C). By contrast, there was no difference in the intranodal distribution of CXCR3-deficient T_{CM} and T_N (Figure S3B), suggesting that CXCR3 is not involved in the

(I) Micrographs showing the distribution of adoptively transferred Ag-specific (P14) and nonspecific (OT-I) T_{CM} in popLNs 8 hr after LCMV infection.
(J) Percentage of T_{CM} in indicated LN compartments.
(K) CD45.2$^+$ mice were adoptively transferred with 10,000–50,000 CD45.1$^+$ P14 T_N and were subsequently infected with LCMV s.c. into footpads. Percentage of CD45.1$^+$ cells in LN cross-sections within indicated compartments. Scale bars, 200 μm in (A) and (C), 100 μm in (B), and 150 μm in all other micrographs.
*$p < 0.05$, **$p < 0.01$, and ***$p < 0.001$. Error bars represent mean ±SEM. See also Figure S2 and Movie S3.

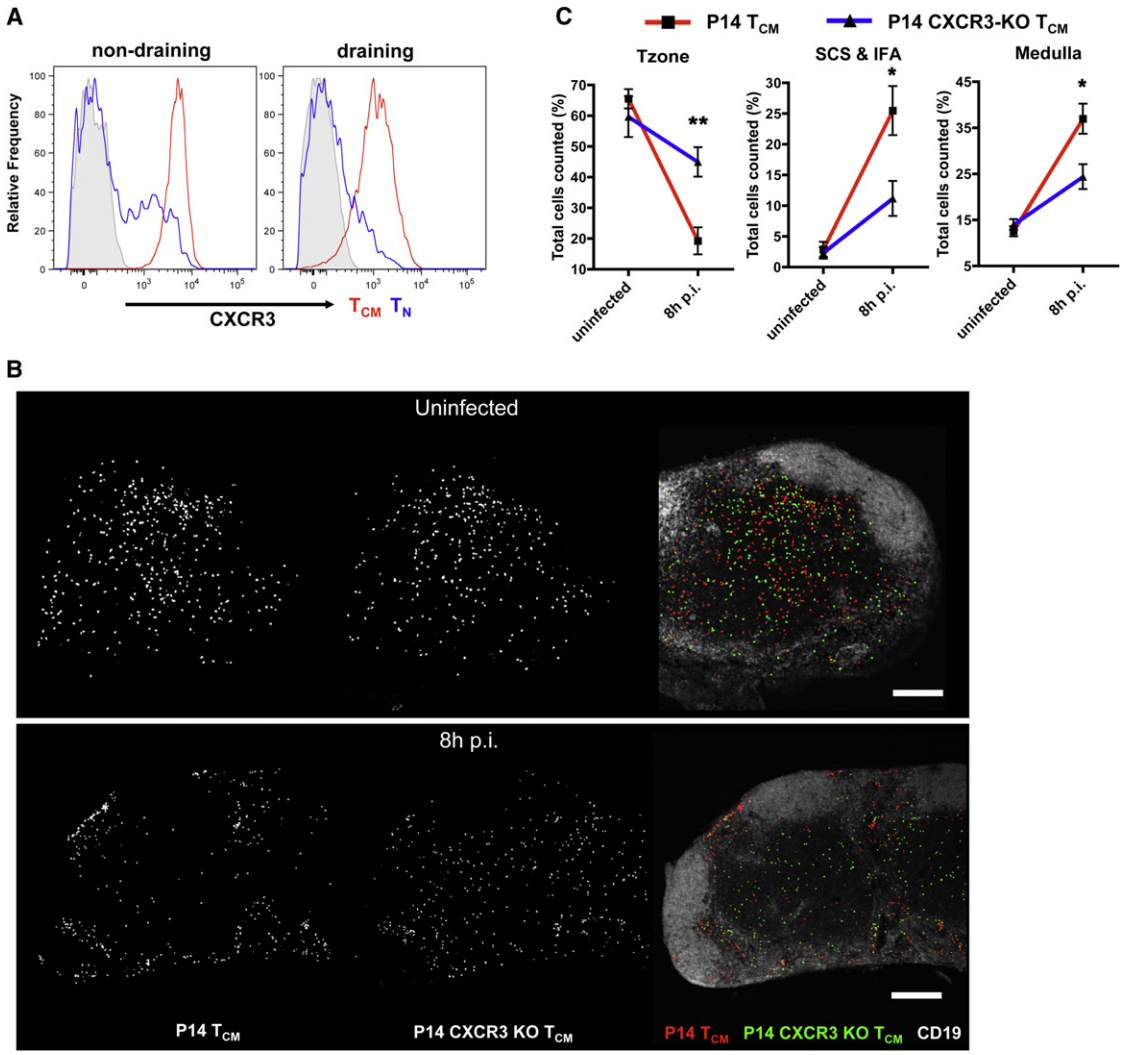

Figure 3. CXCR3 Promotes Viral-Infection-Induced T_{CM} Redistribution in LNs

(A) CXCR3 expression on P14 T_N and T_{CM} in nondraining and draining popLNs 8 hr after footpad infection with LCMV.

(B) Micrographs showing the distribution of adoptively transferred P14 T_{CM} and P14 CXCR3-KO T_{CM} at rest or 8 hr after LCMV infection. Scale bars, 150 μm.

(C) Percentage of P14 T_{CM} and P14 CXCR3-KO T_{CM} in within indicated LN compartments. n = 3.

*$p < 0.05$ and **$p < 0.01$. Error bars represent mean ±SEM. See also Figure S3.

subtle redistribution of T_N, even though a fraction of T_N stained weakly with anti-CXCR3 monoclonal antibody (mAb) (Figure 3A).

CXCR3 Ligands in LCMV-Infected LNs

Next, we sought to characterize the expression of CXCR3 ligands in LNs during a primary or secondary response against LCMV. CXCL9 and CXCL10 messenger RNA (mRNA) levels were measured in popLNs of four groups: (1) uninfected mice; (2) mice infected in a footpad with LCMV for 7 hr ("primary infection"); (3) mice that had been infected with LCMV 25 days earlier and had cleared the virus ("no recall"); and (4) mice infected with LCMV 25 days earlier and rechallenged with LCMV for 7 hr ("secondary infection").

Interestingly, CXCL10 was strongly induced during both primary and secondary infection, whereas CXCL9 was exclusively upregulated during secondary responses (Figure 4A). Thus, we asked whether CXCL9 induction required Ag-specific memory. To this end, we compared the expression of CXCL9 and CXCL10 in mice that had been infected with either LCMV or VSV and 25 days later received a second infection with LCMV. At 7 hr after rechallenge, both CXCL9 and CXCL10 mRNA levels were significantly higher in mice that had previously encountered LCMV, whereas CXCL9 was not detected in LCMV-naive LNs regardless of their previous exposure to VSV (Figure 4B). We conclude that pre-existing antiviral memory is needed to induce CXCL9, but not CXCL10.

Because CXCL9 and CXCL10 are both IFNγ inducible (Farber, 1990; Luster et al., 1985), we tested how IFNγ blockade affects their expression during secondary LCMV infection (Figure 4C). CXCL9 was nearly abrogated by anti-IFNγ treatment, whereas

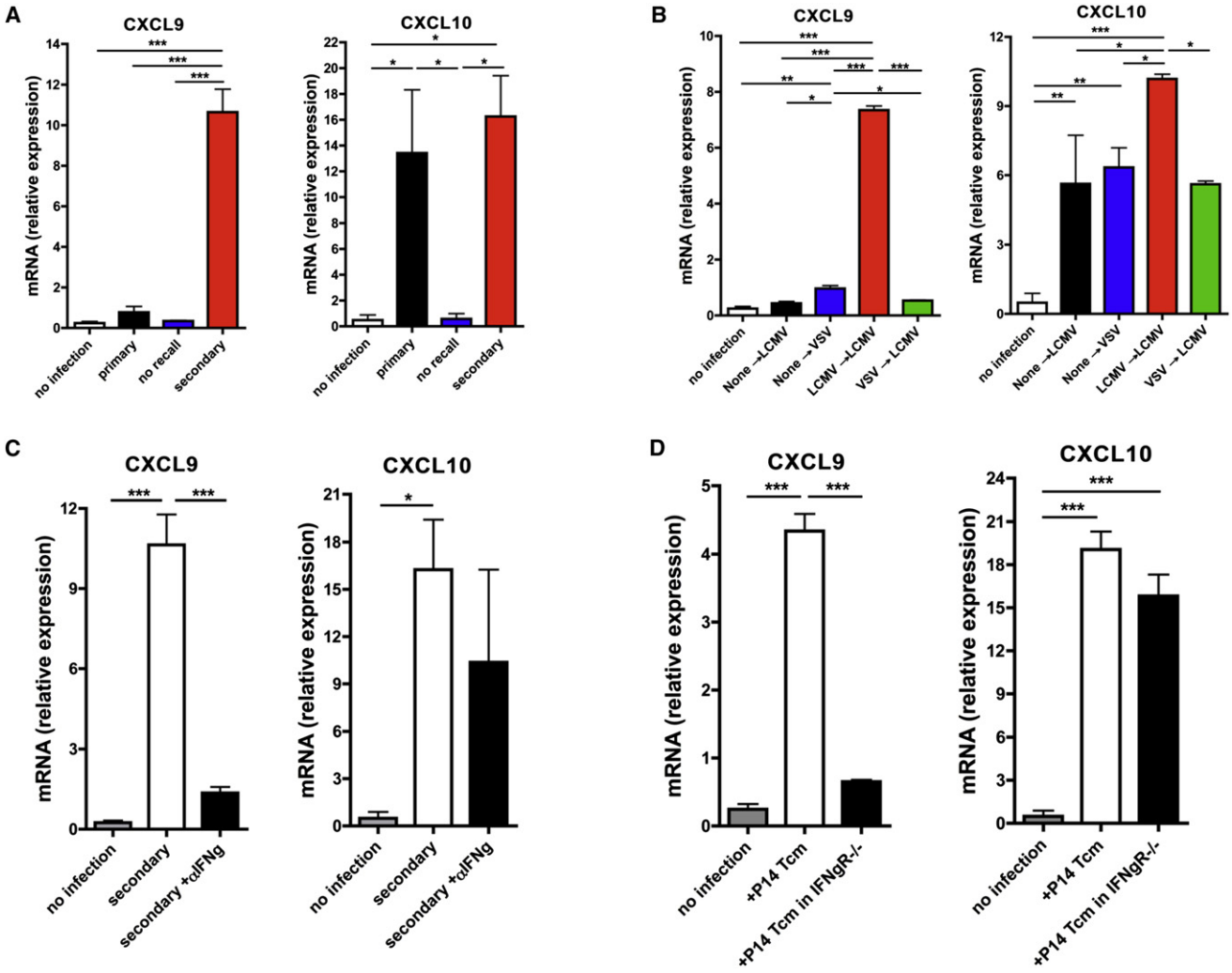

Figure 4. CXCR3 Ligands in LCMV-Infected LNs

(A) CXCL9 and CXCL10 mRNA expression measured by qPCR in popLN of the following: uninfected mice, mice infected with LCMV for 7 hr ("primary"), mice infected with LCMV 25 days earlier ("no recall"), and mice infected with LCMV 25 days earlier and rechallenged with LCMV for 7 hr ("secondary").

(B) CXCL9 and CXCL10 mRNA expression in popLNs of mice that were left uninfected, infected with LCMV or VSV only once, or reinfected with LCMV at day 25 after primary infection with VSV or LCMV.

(C) CXCL9 and CXCL10 mRNA expression in popLNs upon secondary LCMV infection, with or without anti-IFNγ mAb treatment.

(D) CXCL9 and CXCL10 mRNA expression in popLNs of WT or *IFNγR*$^{-/-}$ mice adoptively transferred with P14 T_{CM} and subsequently infected with LCMV (7 hr). All values were normalized to HPRT levels.

*p < 0.05, **p < 0.01, and ***p < 0.001 (one-way analysis of variance [ANOVA] Newman-Keuls multiple comparison test). Error bars represent mean ±SEM.

CXCL10 was minimally affected, suggesting that IFNγ secretion by reactivated virus-specific T_{CM} is necessary to induce the former, but not the latter. Indeed, adoptive transfer of LCMV-specific P14 T_{CM} into naive wild-type (WT) hosts was sufficient to induce CXCL9 expression after LCMV challenge (Figure 4D). This CXCL9 response to LCMV was absent when P14 T_{CM} were transferred to IFNγ-receptor-deficient (*IFNγR*$^{-/-}$) recipients, whereas CXCL10 was still upregulated, albeit at a somewhat reduced level. Together, these results indicate that CXCL9 depends strictly on IFNγ produced by reactivated memory T cells, whereas CXCL10 may be boosted by IFNγ, but a viral infection can induce CXCL10 independently of IFNγ.

Type I Interferon Initiates T_{CM} Relocalization via Induction of CXCL10

We surmised that CXCL10 was induced by an early innate signal triggered by the incipient infection. A likely candidate was type I interferon (IFN-I), which is rapidly produced in LNs undergoing viral infections and can induce CXCR3 ligands (Müller et al., 1994). Indeed, LCMV infection did not induce CXCL10 in animals treated with a blocking mAb against the IFN-I receptor (IFNαR1; Figure 5A). By contrast, CXCL10 levels were unaffected in *IFNγR*$^{-/-}$ LNs undergoing a primary LCMV infection, which is consistent with the finding that anti-IFNγ and IFNγR deficiency have little impact on CXCL10 during secondary responses

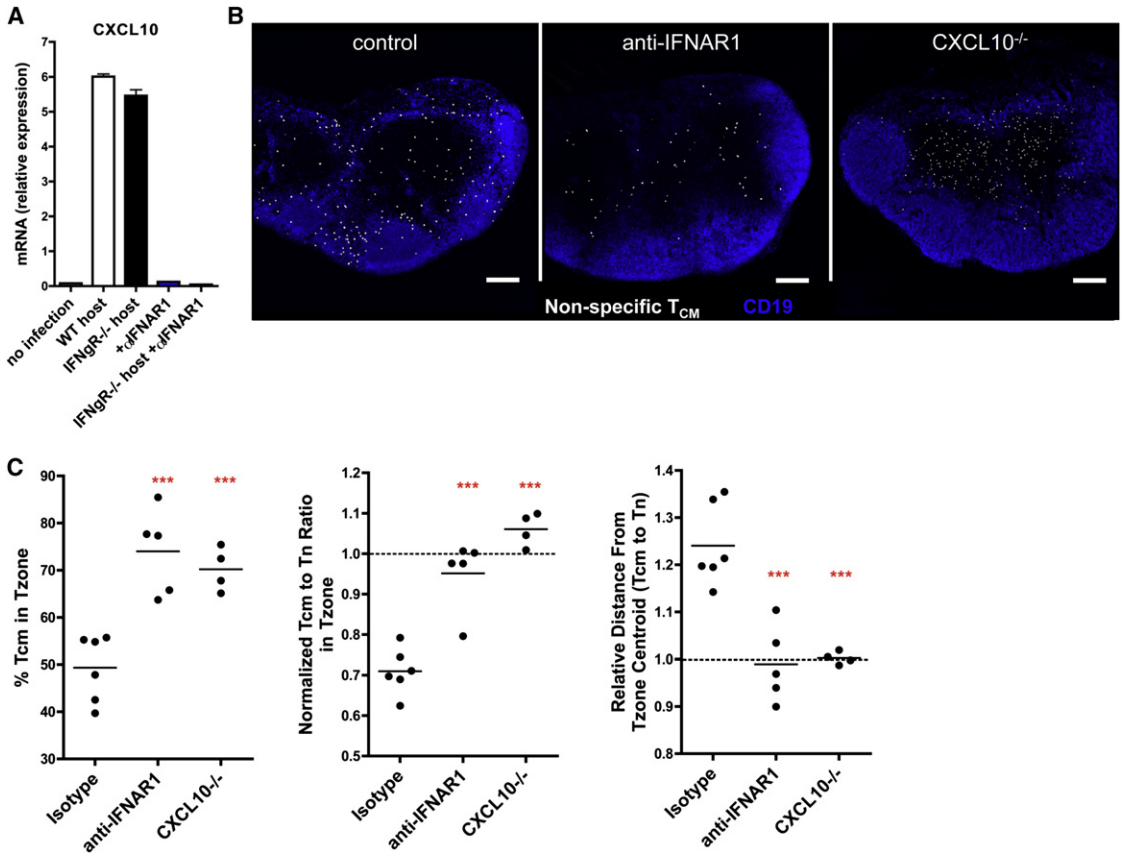

Figure 5. Type I Interferon Initiates T_{CM} Relocalization via Induction of CXCL10

(A) CXCL10 mRNA expression in popLN of WT or *IFNγR*$^{-/-}$ mice 7 hr after footpad LCMV infection, with or without anti-IFNαR1 mAb treatment.

(B) Micrographs showing the distribution of adoptively transferred nonspecific T_{CM} in popLNs of *CXCL10*$^{-/-}$ mice (right) and of WT mice injected with isotype control mAb (left) or anti-IFNαR1 mAb (middle). LNs were dissected 8 hr after footpad LCMV infection. Scale bars, 150 μm.

(C) Percentage of T_{CM} in the T cell area (left). Ratio of T_{CM} to T_N in the T cell area, normalized by the total T_{CM} to T_N ratio in LN cross-section (middle). The ratio of the median distance from centroid of the T cell area to T_{CM} to the median distance from the centroid to T_N (right).

***p < 0.001. Error bars represent mean ±SEM.

(Figures 4C and 4D). Together, these results imply that the rapid production of IFN-I upon viral infection induces CXCL10, which then serves as a chemoattractant that precipitates the exodus of CXCR3$^+$ T_{CM} from the T cell zone.

To test this idea, we compared the LCMV-induced redistribution of T_{CM} versus T_N in WT and *CXCL10*$^{-/-}$ mice in the presence and absence of anti-IFNαR1. We used nonspecific T_{CM} here to avoid potentially confounding effects of Ag-driven IFNγ production. Consistent with the concept that IFN-I is needed for CXCL10 induction, T_{CM} peripheralization upon LCMV infection was markedly inhibited in anti-IFNαR1-treated mice (Figures 5B and 5C). Furthermore, in *CXCL10*$^{-/-}$ mice, the distribution of T_{CM} and T_N remained virtually identical, indicating that the lack of T_{CM} peripheralization after IFNαR1 blockade was due to compromised CXCL10 induction.

IFNγ Production by T_{CM} Induces CXCL9 in Stromal Cells, Macrophages, and Monocytes

We next examined the role of CXCL9, which was only induced during secondary responses (Figure 6A). The largest CXCL9$^+$ population was CD11b$^+$Gr-1$^+$ leukocytes, but CD169$^+$CD11b$^+$ Gr-1$^-$ macrophages, CD11c$^+$ DCs, and CD45$^-$gp38$^+$ stromal cells also expressed CXCL9 (Figures S4A and S4B). The same pattern of CXCL9 expression was also seen in naive LCMV-infected recipients of P14 T_{CM}, but LCMV did not induce CXCL9 in *IFNγR*$^{-/-}$ recipients of P14 T_{CM} or in WT recipients of OT-I T_{CM} or *IFNγ*$^{-/-}$xP14 T_{CM} (Figure 6B).

LCMV infection caused a substantial increase in CD11b$^+$Gr-1$^+$ myeloid cells within 8 hr after viral challenge. This effect was apparent in naive animals (~10-fold increase) and was further exacerbated in previously immunized mice (~30-fold increase; Figure S4C). These newly recruited cells consisted of a minor CD11b^{hi}Gr-1^{hi} and a major CD11b$^+$Gr-1^{int} subset. Both subsets were depleted when mice were injected i.v. with clodronate liposomes (CLLs; Figure S4D), a procedure that depletes circulating monocytes, but not LN macrophages (Tacke et al., 2006). This suggests that peripheral LCMV infection is a potent stimulus for the recruitment of circulating monocytes to LNs. Although LCMV infection alone was sufficient for monocyte recruitment to LNs, the newly recruited cells produced CXCL9 only when

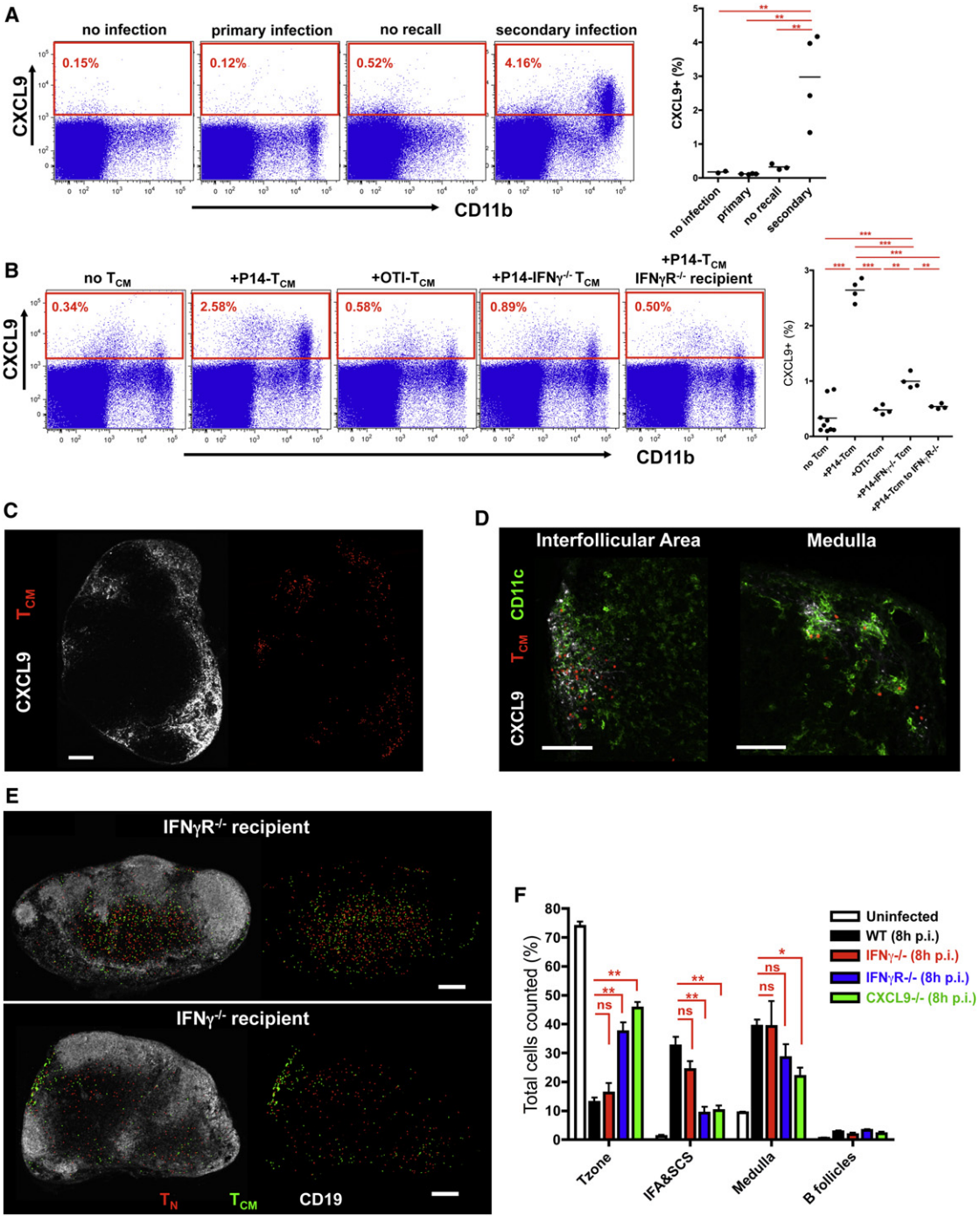

Figure 6. Ag-Triggered IFNγ Production by T_{CM} Induces CXCL9 and Promotes T_{CM} Peripheralization

(A) CXCL9 expression in popLN of uninfected mice, mice infected in a footpad with LCMV for 7 hr ("primary"), mice infected with LCMV 25 days earlier ("no recall"), and mice infected with LCMV for 25 days and rechallenged with LCMV for 7 hr ("secondary").

(B) CXCL9 expression measured by FACS in popLN of the following: control mice (no T_{CM}), WT mice adoptively transferred with P14 T_{CM}, nonspecific (OT-I) T_{CM} or P14 × *IFNγ*$^{-/-}$ T_{CM}, and *IFNγR*$^{-/-}$ mice transferred with P14 T_{CM}. Analysis was performed 8 hr after footpad LCMV infection. One-way ANOVA Newman-Keuls multiple comparison test was used.

(C) Micrograph showing the distribution of T_{CM} and CXCL9 in LCMV-infected popLN (8 hr). Scale bar, 150 μm.

(D) Micrograph showing the distribution of T_{CM}, CXCL9, and CD11c^{+} DCs in the IFA and medulla of LCMV-infected popLN (8 hr). Scale bars, 100 μm.

(E) Micrographs showing the distribution of P14 T_{CM} and T_N in LCMV-infected popLNs of *IFNγR*$^{-/-}$ mice or *IFNγ*$^{-/-}$ mice. Scale bars, 150 μm.

(F) Percentage of P14 T_{CM} within indicated LN compartments. n = 4.

**p < 0.01 and ***p < 0.001. Error bars represent mean ±SEM. See also Figures S4, S5, and S6.

the LNs contained also endogenous or adoptively transferred LCMV-specific T_{CM} (data not shown), suggesting that T_{CM}-derived IFNγ is required to induce CXCL9 in inflammatory monocytes. Only the $CD11b^+CD169^-Gr\text{-}1^{int}$ subset (as well as ~40% of $CD11b^+CD169^+Gr\text{-}1^-$ resident macrophages) produced CXCR9, but not the $CD11b^{hi}Gr\text{-}1^{hi}$ fraction, which also expressed CD169 (Figure S5).

CXCL9 Promotes T_{CM} Peripheralization and Ag Encounter

Fluorescence-activated cell sorting (FACS) analysis of permeabilized LN stromal cells revealed that ~20% of $CD45^-$ cells contained low levels of intracellular CXCL9 upon primary LCMV infection. By contrast, upon secondary infection, >80% of stromal cells were strongly positive (Figure S6A), and ~15% could be stained with anti-CXCL9 without permeabilization, indicating that some stromal cells displayed CXCL9 on their surface, providing a guidance cue for T_{CM} peripheralization. Indeed, immunostaining of frozen LN sections demonstrated that CXCL9 was associated with the ERTR-7^+ stromal network in the IFA and the medulla and within some $CD11b^+$ cells in the same regions (Figures 6C, S6B, and S6C). Furthermore, there was a strong correlation between intranodal T_{CM} distribution and $CXCL9^+$ immunoreactivity.

The LN regions where CXCL9 was expressed contained not only T_{CM}, but also numerous $CD11c^+$ cells (Figure 6D), suggesting that CXCL9 may promote encounters of viral Ag-presenting cells with T_{CM}, which may in turn produce IFNγ to foster further recruitment of T_{CM} via CXCL9. Indeed, the fraction of T_{CM} that remained in the T cell area upon infection was significantly larger in $IFN\gamma R^{-/-}$ mice than in WT (Figures 6E and 6F), despite a partial peripheralization of T_{CM}, presumably in response to IFN-I-driven CXCL10. Moreover, T_{CM} peripheralization was also impaired in $CXCL9^{-/-}$ recipients (Figures 6F and S6D). Thus, although CXCL10 alone can promote the initial formation of T_{CM} contacts with APCs in $IFN\gamma R^{-/-}$ hosts, T_{CM} peripheralization remains suboptimal in the absence of IFNγ-induced CXCL9. Again, the prerequisite source of IFNγ was the T_{CM} themselves because adoptive transfer of IFNγ-competent T_{CM} into $IFN\gamma^{-/-}$ hosts was sufficient to induce T_{CM} relocalization.

CXCR3 Deficiency Delays T_{CM} Recall Responses

Finally, we asked how CXCR3 signaling affects the kinetics of T_{CM} activation upon LCMV rechallenge. We compared the activation kinetics of P14 T_N and T_{CM} to P14 CXCR3-KO T_{CM}. When P14 T_{CM} and P14 CXCR3-KO T_{CM} were activated with anti-CD3/anti-CD28 in vitro, both subsets upregulated activation markers and produced IFNγ with similar kinetics, whereas T_N responded more slowly (Figures 7A and 7B), suggesting that CXCR3 deficiency does not impair the cell-intrinsic capacity of T_{CM} to respond rapidly to rechallenge. However, when the cells were adoptively transferred and analyzed in LNs upon challenge with LCMV, the early activation of CXCR3-KO T_{CM} was markedly delayed.

We next asked whether CXCR3 signaling affects the capacity of T_{CM} to clear cognate virus. To address this, LCMV titers in LNs were determined by measuring mRNA levels of LCMV. To this end, we adoptively transferred an equal number (5×10^5) P14 T_N or T_{CM} or P14 CXCR3-KO T_{CM} into groups of mice and infected the recipients' footpads with LCMV. By 72 hr after infection, LCMV levels were significantly lower in draining LNs of mice injected with P14 T_{CM} as compared to animals injected with P14 CXCR3-KO T_{CM} or P14 T_N (Figure 7C). To confirm this result, we measured intranodal LCMV titers as the infectivity of LN homogenates for cultured fibroblasts (Battegay et al., 1991). Consistent with the quantitative PCR (qPCR) results, LN homogenates from P14 T_{CM} recipients contained significantly fewer focus-forming units than recipients of P14 CXCR3-KO T_{CM} (Figure 7D). Collectively, these results indicate that the CXCR3 pathway accelerates the encounter of viral Ag by T_{CM}, which is critical to enhance the efficiency of antiviral host defense during recall responses.

DISCUSSION

Memory T cells are composed of multiple subsets that differ in the type of effector response they mediate and in their migratory properties (Mora and von Andrian, 2006). Among those, T_{CM} are of particular interest because they have a greater capacity than T_{EM} to persist in vivo, and they are also more efficient at mediating protective immunity because they have superior proliferative potential (Wherry et al., 2003). However, most previous studies of T_{CM} have evaluated their activity at the population level and in settings in which Ag exposure was either systemic or restricted to peripheral tissues (Gil-Cruz et al., 2012; Wherry et al., 2003). Thus, although T_{CM} are defined by their capacity to recirculate through LNs, the precise function of T_{CM} in those organs and the mechanisms by which they differ from T_N have been unclear.

To fill this knowledge gap, we have compared how T_{CM} and T_N respond in LNs to a model virus, LCMV, which requires a CTL response for efficient clearance (Byrne and Oldstone, 1984). Unexpectedly, our experiments revealed that both T cell subsets responded similarly when they encountered the immunodominant peptide of LCMV on mature DCs within the T cell area. The acquisition of activation markers, onset, and magnitude of Ag-driven proliferation and the interaction dynamics with DCs were all roughly equivalent. The only clear difference between T_N and T_{CM} responses to Ag-pulsed DCs was a more vigorous IFNγ response by the latter. By contrast, when LNs were instead infected with lymph-borne virus, activation and proliferation, as well as IFNγ production, occurred more rapidly in T_{CM} than in T_N.

The accelerated response of T_{CM} to LCMV infection depended upon a cascade of cytokines and chemokines, particularly ligands for CXCR3, which selectively guided T_{CM} migration toward infected cells (Figure S7). Following LCMV challenge, the initial signal for T_{CM} redistribution was triggered as soon as SCS and medullary macrophages became infected with the lymph-borne virus because the infected cells rapidly released IFN-I. This, in turn, triggered local production of the inflammatory chemokine CXCL10, which diffused from the LN periphery toward the deep cortex, establishing a concentration gradient that T_{CM}, but not T_N, could follow. By tracking this chemoattractant cue, some T_{CM} gained access to the LN periphery, where they encountered viral Ag-presenting cells. TCR stimulation then prompted IFN-γ secretion by T_{CM}, which provoked the production of CXCL9 and further amplified the peripheralization

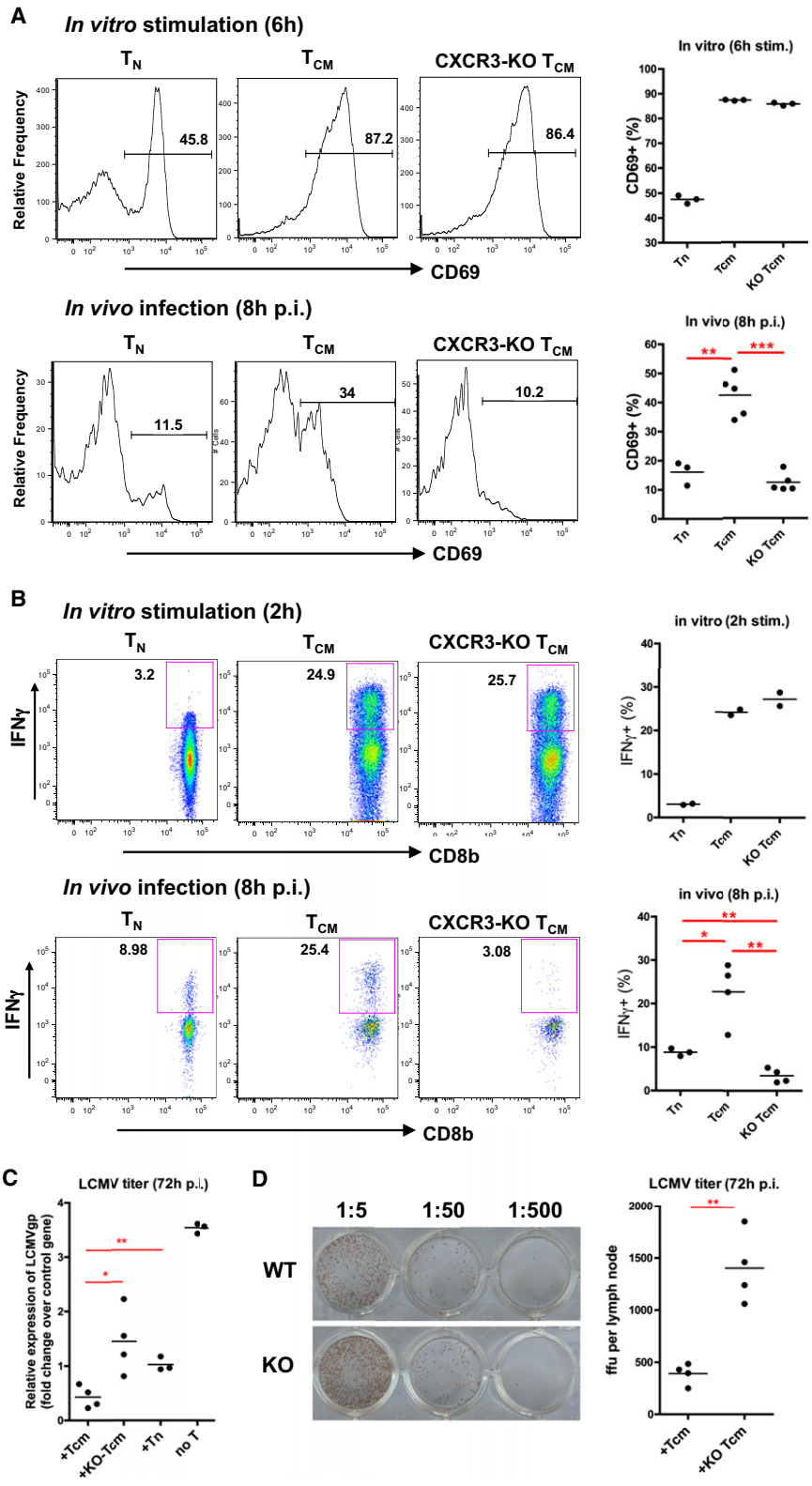

Figure 7. CXCR3 Deficiency in T_{CM} Delays the Recall Response against LCMV Infection

(A and B) P14 T_N, P14 T_{CM}, or P14 CXCR3-KO T_{CM} stimulated in vitro with anti-CD3/CD28 or harvested from popLN 8 hr after footpad infection with LCMV and analyzed for (A) CD69 induction and (B) IFNγ secretion.

(C) LCMV titers measured as LCMV gp mRNA in popLN. Mice received footpad infections without or with prior adoptive transfer of P14 T_N, P14 T_{CM}, or P14 × CXCR3-KO T_{CM}, and titers were measured at 72 hr.

(D) LCMV titers measured by focus assay in LCMV-infected popLNs of recipients of P14 T_{CM} or P14 CXCR3-KO T_{CM} 72 hr after footpad infection. *$p < 0.05$, **$p < 0.01$, and ***$p < 0.001$. Error bars represent mean ±SEM. See also Figure S7.

of T_{CM}. The result was the rapid exodus of nearly all Ag-specific T_{CM} from the T cell area toward the SCS and medulla. CXCR3-deficient T_{CM} failed to peripheralize and could not provide enhanced protection against LCMV rechallenge as compared to T_N, indicating that CXCR3 is a key determinant of T_{CM} function, at least in LNs undergoing an acute LCMV infection.

These results confirm and expand the concept that the migratory properties of T_{CM} are a critical determinant of their protective capacity. In addition to their sustained LN tropism, a feature that they share with T_N and that sets them apart from T_{EM} (Sallusto et al., 1999; Weninger et al., 2001), we show that T_{CM} can uniquely follow intranodal distress signals to migrate to the most vulnerable regions of LNs where lymph-borne pathogens are first encountered and that are poorly accessible to T_N and T_{EM}. This capacity of T_{CM} may be particularly relevant for intracellular pathogens such as LCMV, which is highly proliferative and elicits poor neutralizing antibody responses and, therefore, requires rapid cell-mediated protection (Buchmeier et al., 1980). Although it is unclear whether the CXCR3 dependence of T_{CM} is singularly relevant for LCMV in LNs or applies also to other infectious settings, it seems likely that intranodal T_{CM} migration has a broad role in antiviral host protection. This prediction appears inevitable if we consider the immunological, microanatomical, and biophysical features that constrain or promote viral dissemination in immunized hosts.

When the body's surface barriers are breached by a previously encountered pathogen, the ensuing recall response depends on many factors, for example, the frequency and differentiation status of host memory cells, the presence of neutralizing antibodies, the pathogen's host cell tropism, its expression of ligands for pathogen-associated molecular pattern receptors, proliferative capacity, and possibly even the size of the microbe. Viruses that are not rapidly neutralized by humoral responses may infect host cells at the site of entry, where they must be eliminated by tissue-tropic T_{EM}, T_{Eff}, or NK cells (Irla et al., 2010; Masopust et al., 2001; Paust et al., 2010). Owing to their small size, most virions can freely access the lymph drainage system and are transported within minutes to downstream LNs (Junt et al., 2007). Lymph-borne viruses whose host cell tropism is restricted to peripheral tissues (e.g., influenza or herpes simplex virus [HSV]) are captured by phagocytes without causing intranodal infection (Gonzalez et al., 2010), whereas viruses with broad host cell tropism (such as VSV or LCMV) or with specific tropism for LN-resident cells may establish intranodal infections. It seems likely that T_{CM} are particularly critical for protection against reinfection with those viruses (and other intracellular pathogens [Chtanova et al., 2009]) that can become lymph borne and invade LN-resident target cells.

Among all LN resident cells, macrophages within the SCS and medulla are arguably the most exposed to infectious viruses because they are constantly bathed in lymph fluid. All lymph-borne viruses that have been tested to date are efficiently trapped in LNs by SCS and/or medullary macrophages, which is an important mechanism to prevent systemic pathogen dissemination (Gonzalez et al., 2010; Junt et al., 2007). Thus, LN macrophages often become the first site of intranodal viral replication. Recent findings indicate that the continuous exposure of SCS macrophages to surface-expressed lymphotoxin on follicular B cells provides a differentiation signal that renders this macrophage subset particularly susceptible to infection with VSV, which triggers a protective IFN-I response (Moseman et al., 2012). Unlike the SCS subset, medullary macrophages, which are not in contact with follicular B cells, usually remain uninfected by VSV. Interestingly, the present results indicate that medullary macrophages are not resistant to LCMV infection but, together with the SCS subset, represent the first target cells for intranodal LCMV replication. The mechanism for this differential vulnerability of medullary macrophages remains to be elucidated.

Irrespective of the location or mechanism of macrophage invasion by LCMV, cytotoxic effector cells can only eliminate the viral threat if they gain quick access to infected cells. Because macrophages themselves are poorly migratory and the macrophage-rich lymph conduits are remote from the central T cell area, virus-specific T cells must have the means for directional migration toward viral Ag-presenting macrophages in the outermost regions of the LN. Our results show that the infected macrophages promote their own detection by sending out molecular distress signals, CXCL9 and CXCL10, that attract T_{CM}. Of note, LCMV challenge not only provoked rapid peripheralization of T_{CM} but also mobilized several other leukocyte subsets, including myeloid cells and, to some extent, even T_N. For example, virally infected macrophages attract plasmacytoid DCs (pDCs), which usually reside in the deep cortex and can provide an additional source of IFN-I (Iannacone et al., 2010). Because pDCs express CXCR3 (Cella et al., 1999), it seems plausible that their recruitment is accomplished by the same chemoattractant pathway that promotes T_{CM} peripheralization.

Consistent with previous studies on T cell responses to vaccinia virus or VSV (Hickman et al., 2008) or *Toxoplasma gondii* (Chtanova et al., 2009), which also infect LN macrophages, infection with LCMV induced a redistribution of T_N toward the LN periphery, albeit with lower efficiency and slower kinetics than T_{CM}. Neither the identity nor the source of the guidance cue for intranodal T_N redistribution are known, but it should be noted that the inflammatory milieu in reactive LNs causes $CD8^+$ T_N to acquire CCR5, a receptor for inflammation-induced chemokines released by activated DCs (Castellino et al., 2006; Hickman et al., 2011). Whatever the signal(s) for T_N peripheralization, it is possible that the same pathway or pathways also contribute to T_{CM} redistribution.

Besides altering the migratory properties of LN-resident T cells, LCMV infection also caused a profound increase in myeloid cells in LNs. Some of these cells could have accessed LNs via afferent lymphatics; however, given the rapidity at which myeloid cells appeared after LCMV exposure (<8 hr), they were more likely recruited via HEVs from the blood. Two discrete myeloid subsets were evident—a larger $Gr\text{-}1^+CD11b^+$ population reflecting inflammatory monocytes and a minor subset that was $Gr\text{-}1^{hi}$ $CD11b^{hi}$ and $CD169^{+/low}$. A small fraction of circulating monocytes/macrophages, as well pDCs, express CXCR3 and could have been recruited to LCMV-infected LNs by inflammation-induced CXCL10 (Janatpour et al., 2001; Yoneyama et al., 2004). However, most circulating monocytes do not express CXCR3. Their recruitment could have been mediated by CCL2, a chemokine that is generated at sites of inflammation and is transported via the lymph to HEVs in draining

LNs, where it then promotes homing of $CCR2^+$ monocytes (Palframan et al., 2001). Interestingly, the accumulation of myeloid cells in LNs was significantly enhanced during secondary responses. Although neither T_{CM}-derived IFNγ nor host cell expression of IFNγR was required for the recruitment of myeloid cells, T_{CM}-derived IFNγ was essential to prompt the newly recruited monocytes and other cells in the LN periphery to produce CXCL9.

Together, these results suggest a scenario whereby T_{CM} are rapidly attracted toward infected macrophages by IFN-I-induced CXCL10. Upon encounter of cognate Ag, T_{CM} accelerate the recruitment of myeloid cells. Simultaneously, IFNγ release from reactivated T_{CM} induces the production of CXCL9 from several different cellular sources, particularly from monocytes. The peripheral confinement of CXCL9-producing cells during secondary responses suggests that the newly recruited monocytes, after entering the LN from HEV in the T cell area, must first migrate toward the outer cortex and medulla. Here, they encounter IFNγ released by T_{CM}, which induces the secretion of CXCL9 into the interstitial space. CXCL9 then binds to the cortical stroma cell network on which immobilized chemokines provide haptotactic guidance cues that may facilitate the peripheralization of additional T_{CM} toward the LN periphery. Although CXCL9 was important for T_{CM} migration to IFA, SCS, and medulla, CXCL9 production in the latter region may not be absolutely dependent upon IFNγ because medullary accumulation of T_{CM} in *IFNγR*$^{-/-}$ hosts was only modestly affected.

At later stages of the infection, migratory DCs begin to arrive in LNs carrying a second wave of viral Ag from the periphery. These cells must cross the SCS to migrate toward the T cell area (Alvarez et al., 2008). During this process, DCs pass across the macrophage-rich layer containing viral Ag-specific T_{CM} that had been previously attracted via CXCR3. Thus, the geographic difference in T cell subset localization upon LCMV infection provides an advantage to T_{CM} versus T_N to initiate communications with DCs. Because T_N and T_{CM} interacted similarly with Ag-pulsed DCs in the deep cortex when their arrival in LNs was synchronized, whatever kinetic advantage T_{CM} may possess over T_N in obtaining information from DCs appears to result from their preferential capacity to peripheralize. This allows them to meet the incoming DCs halfway, whereas T_N must await the arrival of DCs in the deep cortex.

Our findings demonstrate how two chemokines sharing the same receptor synergize to enable T_{CM} function during distinct phases of an antiviral recall response. The sequential appearance of CXCL10 followed by CXCL9 is consistent with previous observations in settings of viral infection and allotransplantation (Hancock et al., 2001; Medoff et al., 2006) and can be explained by the fact that the respective genes are differentially responsive to cytokines, with CXCL9 being strictly dependent upon IFNγ, whereas CXCL10 is also inducible by IFN-I (Groom and Luster, 2011). The differential dependence of CXCL9 and CXCL10 on a secondary T cell response to recall Ag was equally observed in settings in which T cell memory had been induced endogenously and in naive recipients of ex-vivo-differentiated T_{CM}, suggesting that adoptive transfer of IL-15-induced T_{CM} is an appropriate approach to study this process. It should be noted that the C57BL/6 strain used here has a frame shift mutation in the gene for CXCL11, a third ligand for CXCR3 (Sierro et al., 2007). Thus, the contribution of individual CXCR3 agonists to T_{CM} function could be even more complex in animals that express functional CXCL11, including humans. In addition, CXCR3 is implicated in other aspects of antiviral immunity, including the regulation of effector and memory cell differentiation (Hu et al., 2011; Kohlmeier et al., 2009; Kurachi et al., 2011) and the recruitment of circulating T_{EFF} to inflamed LNs via HEV (Guarda et al., 2007). However, the latter mechanism does not appear to contribute in the present setting because WT and CXCR3-KO T_{CM} home similarly to LCMV-infected LNs, at least during the first 18 hr after infection (data not shown), presumably because blood-borne T_{CM} express classical LN homing receptors that may be redundant with CXCR3. Thus, the present findings highlight yet another critical role for CXCR3 and its ligands and indicate that preferred access to recall Ag, rather than differential interaction dynamics with DCs, is a critical determinant of protective CD8 T cell memory in LNs.

EXPERIMENTAL PROCEDURES

Mice

C57BL/6 mice were purchased from Charles River. P14 and OT-I mice, which carry a transgenic TCR specific for LCMV glycoprotein (Pircher et al., 1989) and ovalbumin (Hogquist et al., 1994), respectively, were purchased from Taconic Farms. CXCR3-KO, *IFNγR*$^{-/-}$, and *IFNγ*$^{-/-}$ mice were purchased from Jackson Laboratory. *CXCL9*$^{-/-}$ mice were kindly provided by J.M. Farber (NIAID) (Park et al., 2002). Both *CXCL9*$^{-/-}$ and *CXCL10*$^{-/-}$ (Dufour et al., 2002) mice were backcrossed into C57BL/6 for ≥9 generations at MGH. Mice were housed in a specific pathogen-free barrier facility. All experiments were in accordance with NIH guidelines and were approved by the Institutional Animal Committees of Harvard Medical School.

Viruses and Infections

LCMV Armstrong and VSV Indiana were propagated and purified as described (Junt et al., 2007; von Herrath and Whitton, 2001). Mice were infected with LCMV Armstrong (10^4 focus-forming units [FFU]) or VSV Indiana (10^4–10^5 plaque-forming unit [PFU]) by subcutaneous injection into the hind footpad. LCMV titers were measured by quantitative PCR or focus assay as described (Battegay et al., 1991). LCMV-EGFP was kindly provided by J.C. de la Torre. All infectious work was performed in designated BL2+ workspaces, in accordance with institutional guidelines, and was approved by the Harvard Committee on Microbiological Safety.

Generation of Memory CD8 T Cells

$CD45.2^+$ B6 mice were injected with 10,000–50,000 $CD45.1^+$ P14 T_N i.v., followed by infection with LCMV into footpads. After ~25 days, $CD45.1^+$ memory cells in the draining popLNs were detected by using an anti-CD45.1 antibody. Generation of memory-like CD8 T cells in vitro was performed as described (Manjunath et al., 2001). Splenocytes from TCR transgenic mice were incubated with cognate peptides (New England Peptide) at 37°C for 1 hr. Cells were washed and cultured for 2 days. Cells were split every 2 days, and 20 ng/ml of recombinant human IL-15 (R&D) was added into media. After ~9 days of culture, cells were tested for the expression of CD8, CD44, CD69, CD62L, and CXCR3 by FACS.

Confocal Microscopy

PopLNs were processed for confocal microscopy as described (Junt et al., 2007). LNs incubated overnight in phosphate-buffered l-lysine with 1% paraformaldehyde/periodate (PLP). LNs were then cryoprotected by subsequent incubations in 10%, 20%, and 30% sucrose in PBS at room temperature. LNs were frozen in TBS tissue-freezing media (Triangle Biomedical Sciences)

and were sectioned at 30 μm intervals. Images were acquired with an Olympus Fluoview BX50WI inverted microscope and were analyzed by using Volocity software (Improvision).

Statistical Analyses

Results are expressed as means ±SEM, and means were compared by using a two-tailed t test, unless otherwise indicated. All statistical analyses were performed in Prism Software.

SUPPLEMENTAL INFORMATION

Supplemental Information includes Extended Experimental Procedures, seven figures, and three movies and can be found with this article online at http://dx.doi.org/10.1016/j.cell.2012.08.015.

ACKNOWLEDGMENTS

We thank M. Flynn and Dr. G. Cheng for technical support, M. Perdue for secretarial assistance, and the members of the von Andrian laboratory for helpful discussion. This work was supported by NIH grants AI078897, AI069259 (to U.H.v.A.), 5T32-HL07623-20 (to E.A.M.), and CA069212 (to A.D.L.); a Samsung Scholarship (to J.H.S.); the Armenise-Harvard Foundation (to M.I.); the Canadian Institutes of Health Research (to D.A.); and an Overseas Biomedical Fellowship from the National Health and Medical Research Council of Australia (to J.R.G.).

Received: March 12, 2012
Revised: May 12, 2012
Accepted: August 3, 2012
Published: September 13, 2012

REFERENCES

Alvarez, D., Vollmann, E.H., and von Andrian, U.H. (2008). Mechanisms and consequences of dendritic cell migration. Immunity *29*, 325–342.

Battegay, M., Cooper, S., Althage, A., Bänziger, J., Hengartner, H., and Zinkernagel, R.M. (1991). Quantification of lymphocytic choriomeningitis virus with an immunological focus assay in 24- or 96-well plates. J. Virol. Methods *33*, 191–198.

Buchmeier, M.J., Welsh, R.M., Dutko, F.J., and Oldstone, M.B. (1980). The virology and immunobiology of lymphocytic choriomeningitis virus infection. Adv. Immunol. *30*, 275–331.

Byrne, J.A., and Oldstone, M.B. (1984). Biology of cloned cytotoxic T lymphocytes specific for lymphocytic choriomeningitis virus: clearance of virus in vivo. J. Virol. *51*, 682–686.

Castellino, F., Huang, A.Y., Altan-Bonnet, G., Stoll, S., Scheinecker, C., and Germain, R.N. (2006). Chemokines enhance immunity by guiding naive CD8+ T cells to sites of CD4+ T cell-dendritic cell interaction. Nature *440*, 890–895.

Cella, M., Jarrossay, D., Facchetti, F., Alebardi, O., Nakajima, H., Lanzavecchia, A., and Colonna, M. (1999). Plasmacytoid monocytes migrate to inflamed lymph nodes and produce large amounts of type I interferon. Nat. Med. *5*, 919–923.

Chtanova, T., Han, S.J., Schaeffer, M., van Dooren, G.G., Herzmark, P., Striepen, B., and Robey, E.A. (2009). Dynamics of T cell, antigen-presenting cell, and pathogen interactions during recall responses in the lymph node. Immunity *31*, 342–355.

Dufour, J.H., Dziejman, M., Liu, M.T., Leung, J.H., Lane, T.E., and Luster, A.D. (2002). IFN-gamma-inducible protein 10 (IP-10; CXCL10)-deficient mice reveal a role for IP-10 in effector T cell generation and trafficking. J. Immunol. *168*, 3195–3204.

Emonet, S.F., Garidou, L., McGavern, D.B., and de la Torre, J.C. (2009). Generation of recombinant lymphocytic choriomeningitis viruses with trisegmented genomes stably expressing two additional genes of interest. Proc. Natl. Acad. Sci. USA *106*, 3473–3478.

Farber, J.M. (1990). A macrophage mRNA selectively induced by gamma-interferon encodes a member of the platelet factor 4 family of cytokines. Proc. Natl. Acad. Sci. USA *87*, 5238–5242.

Gebhardt, T., Wakim, L.M., Eidsmo, L., Reading, P.C., Heath, W.R., and Carbone, F.R. (2009). Memory T cells in nonlymphoid tissue that provide enhanced local immunity during infection with herpes simplex virus. Nat. Immunol. *10*, 524–530.

Gil-Cruz, C., Perez-Shibayama, C., Firner, S., Waisman, A., Bechmann, I., Thiel, V., Cervantes-Barragan, L., and Ludewig, B. (2012). T helper cell- and CD40-dependent germline IgM prevents chronic virus-induced demyelinating disease. Proc. Natl. Acad. Sci. USA *109*, 1233–1238.

Gonzalez, S.F., Lukacs-Kornek, V., Kuligowski, M.P., Pitcher, L.A., Degn, S.E., Kim, Y.A., Cloninger, M.J., Martinez-Pomares, L., Gordon, S., Turley, S.J., and Carroll, M.C. (2010). Capture of influenza by medullary dendritic cells via SIGN-R1 is essential for humoral immunity in draining lymph nodes. Nat. Immunol. *11*, 427–434.

Groom, J.R., and Luster, A.D. (2011). CXCR3 ligands: redundant, collaborative and antagonistic functions. Immunol. Cell Biol. *89*, 207–215.

Guarda, G., Hons, M., Soriano, S.F., Huang, A.Y., Polley, R., Martín-Fontecha, A., Stein, J.V., Germain, R.N., Lanzavecchia, A., and Sallusto, F. (2007). L-selectin-negative CCR7- effector and memory CD8+ T cells enter reactive lymph nodes and kill dendritic cells. Nat. Immunol. *8*, 743–752.

Halin, C., Mora, J.R., Sumen, C., and von Andrian, U.H. (2005). In vivo imaging of lymphocyte trafficking. Annu. Rev. Cell Dev. Biol. *21*, 581–603.

Hancock, W.W., Gao, W., Csizmadia, V., Faia, K.L., Shemmeri, N., and Luster, A.D. (2001). Donor-derived IP-10 initiates development of acute allograft rejection. J. Exp. Med. *193*, 975–980.

Henrickson, S.E., and von Andrian, U.H. (2007). Single-cell dynamics of T-cell priming. Curr. Opin. Immunol. *19*, 249–258.

Henrickson, S.E., Mempel, T.R., Mazo, I.B., Liu, B., Artyomov, M.N., Zheng, H., Peixoto, A., Flynn, M.P., Senman, B., Junt, T., et al. (2008). T cell sensing of antigen dose governs interactive behavior with dendritic cells and sets a threshold for T cell activation. Nat. Immunol. *9*, 282–291.

Hickman, H.D., Takeda, K., Skon, C.N., Murray, F.R., Hensley, S.E., Loomis, J., Barber, G.N., Bennink, J.R., and Yewdell, J.W. (2008). Direct priming of antiviral CD8+ T cells in the peripheral interfollicular region of lymph nodes. Nat. Immunol. *9*, 155–165.

Hickman, H.D., Li, L., Reynoso, G.V., Rubin, E.J., Skon, C.N., Mays, J.W., Gibbs, J., Schwartz, O., Bennink, J.R., and Yewdell, J.W. (2011). Chemokines control naive CD8+ T cell selection of optimal lymph node antigen presenting cells. J. Exp. Med. *208*, 2511–2524.

Hogquist, K.A., Jameson, S.C., Heath, W.R., Howard, J.L., Bevan, M.J., and Carbone, F.R. (1994). T cell receptor antagonist peptides induce positive selection. Cell *76*, 17–27.

Hu, J.K., Kagari, T., Clingan, J.M., and Matloubian, M. (2011). Expression of chemokine receptor CXCR3 on T cells affects the balance between effector and memory CD8 T-cell generation. Proc. Natl. Acad. Sci. USA *108*, E118–E127.

Iannacone, M., Moseman, E.A., Tonti, E., Bosurgi, L., Junt, T., Henrickson, S.E., Whelan, S.P., Guidotti, L.G., and von Andrian, U.H. (2010). Subcapsular sinus macrophages prevent CNS invasion on peripheral infection with a neurotropic virus. Nature *465*, 1079–1083.

Irla, M., Küpfer, N., Suter, T., Lissilaa, R., Benkhoucha, M., Skupsky, J., Lalive, P.H., Fontana, A., Reith, W., and Hugues, S. (2010). MHC class II-restricted antigen presentation by plasmacytoid dendritic cells inhibits T cell-mediated autoimmunity. J. Exp. Med. *207*, 1891–1905.

Janatpour, M.J., Hudak, S., Sathe, M., Sedgwick, J.D., and McEvoy, L.M. (2001). Tumor necrosis factor-dependent segmental control of MIG expression by high endothelial venules in inflamed lymph nodes regulates monocyte recruitment. J. Exp. Med. *194*, 1375–1384.

Junt, T., Moseman, E.A., Iannacone, M., Massberg, S., Lang, P.A., Boes, M., Fink, K., Henrickson, S.E., Shayakhmetov, D.M., Di Paolo, N.C., et al. (2007).

Subcapsular sinus macrophages in lymph nodes clear lymph-borne viruses and present them to antiviral B cells. Nature *450*, 110–114.

Kaech, S.M., Hemby, S., Kersh, E., and Ahmed, R. (2002). Molecular and functional profiling of memory CD8 T cell differentiation. Cell *111*, 837–851.

Kohlmeier, J.E., Cookenham, T., Miller, S.C., Roberts, A.D., Christensen, J.P., Thomsen, A.R., and Woodland, D.L. (2009). CXCR3 directs antigen-specific effector CD4+ T cell migration to the lung during parainfluenza virus infection. J. Immunol. *183*, 4378–4384.

Kurachi, M., Kurachi, J., Suenaga, F., Tsukui, T., Abe, J., Ueha, S., Tomura, M., Sugihara, K., Takamura, S., Kakimi, K., et al. (2011). Chemokine receptor CXCR3 facilitates CD8(+) T cell differentiation into short-lived effector cells leading to memory degeneration. J. Exp. Med. *208*, 1605–1620.

Luster, A.D., Unkeless, J.C., and Ravetch, J.V. (1985). Gamma-interferon transcriptionally regulates an early-response gene containing homology to platelet proteins. Nature *315*, 672–676.

Manjunath, N., Shankar, P., Wan, J., Weninger, W., Crowley, M.A., Hieshima, K., Springer, T.A., Fan, X., Shen, H., Lieberman, J., and von Andrian, U.H. (2001). Effector differentiation is not prerequisite for generation of memory cytotoxic T lymphocytes. J. Clin. Invest. *108*, 871–878.

Masopust, D., Vezys, V., Marzo, A.L., and Lefrançois, L. (2001). Preferential localization of effector memory cells in nonlymphoid tissue. Science *291*, 2413–2417.

Medoff, B.D., Wain, J.C., Seung, E., Jackobek, R., Means, T.K., Ginns, L.C., Farber, J.M., and Luster, A.D. (2006). CXCR3 and its ligands in a murine model of obliterative bronchiolitis: regulation and function. J. Immunol. *176*, 7087–7095.

Mempel, T.R., Henrickson, S.E., and Von Andrian, U.H. (2004). T-cell priming by dendritic cells in lymph nodes occurs in three distinct phases. Nature *427*, 154–159.

Miller, M.J., Safrina, O., Parker, I., and Cahalan, M.D. (2004). Imaging the single cell dynamics of CD4+ T cell activation by dendritic cells in lymph nodes. J. Exp. Med. *200*, 847–856.

Mora, J.R., and von Andrian, U.H. (2006). Specificity and plasticity of memory lymphocyte migration. Curr. Top. Microbiol. Immunol. *308*, 83–116.

Moseman, E.A., Iannacone, M., Bosurgi, L., Tonti, E., Chevrier, N., Tumanov, A., Fu, Y.X., Hacohen, N., and von Andrian, U.H. (2012). B cell maintenance of subcapsular sinus macrophages protects against a fatal viral infection independent of adaptive immunity. Immunity *36*, 415–426.

Müller, U., Steinhoff, U., Reis, L.F., Hemmi, S., Pavlovic, J., Zinkernagel, R.M., and Aguet, M. (1994). Functional role of type I and type II interferons in antiviral defense. Science *264*, 1918–1921.

Palframan, R.T., Jung, S., Cheng, G., Weninger, W., Luo, Y., Dorf, M., Littman, D.R., Rollins, B.J., Zweerink, H., Rot, A., and von Andrian, U.H. (2001). Inflammatory chemokine transport and presentation in HEV: a remote control mechanism for monocyte recruitment to lymph nodes in inflamed tissues. J. Exp. Med. *194*, 1361–1373.

Park, M.K., Amichay, D., Love, P., Wick, E., Liao, F., Grinberg, A., Rabin, R.L., Zhang, H.H., Gebeyehu, S., Wright, T.M., et al. (2002). The CXC chemokine murine monokine induced by IFN-gamma (CXC chemokine ligand 9) is made by APCs, targets lymphocytes including activated B cells, and supports antibody responses to a bacterial pathogen in vivo. J. Immunol. *169*, 1433–1443.

Paust, S., Gill, H.S., Wang, B.Z., Flynn, M.P., Moseman, E.A., Senman, B., Szczepanik, M., Telenti, A., Askenase, P.W., Compans, R.W., and von Andrian, U.H. (2010). Critical role for the chemokine receptor CXCR6 in NK cell-mediated antigen-specific memory of haptens and viruses. Nat. Immunol. *11*, 1127–1135.

Pircher, H., Bürki, K., Lang, R., Hengartner, H., and Zinkernagel, R.M. (1989). Tolerance induction in double specific T-cell receptor transgenic mice varies with antigen. Nature *342*, 559–561.

Pulendran, B., and Ahmed, R. (2006). Translating innate immunity into immunological memory: implications for vaccine development. Cell *124*, 849–863.

Rot, A., and von Andrian, U.H. (2004). Chemokines in innate and adaptive host defense: basic chemokinese grammar for immune cells. Annu. Rev. Immunol. *22*, 891–928.

Sallusto, F., Lenig, D., Förster, R., Lipp, M., and Lanzavecchia, A. (1999). Two subsets of memory T lymphocytes with distinct homing potentials and effector functions. Nature *401*, 708–712.

Sierro, F., Biben, C., Martínez-Muñoz, L., Mellado, M., Ransohoff, R.M., Li, M., Woehl, B., Leung, H., Groom, J., Batten, M., et al. (2007). Disrupted cardiac development but normal hematopoiesis in mice deficient in the second CXCL12/SDF-1 receptor, CXCR7. Proc. Natl. Acad. Sci. USA *104*, 14759–14764.

Sprent, J., and Surh, C.D. (2002). T cell memory. Annu. Rev. Immunol. *20*, 551–579.

Tacke, F., Ginhoux, F., Jakubzick, C., van Rooijen, N., Merad, M., and Randolph, G.J. (2006). Immature monocytes acquire antigens from other cells in the bone marrow and present them to T cells after maturing in the periphery. J. Exp. Med. *203*, 583–597.

von Andrian, U.H., and Mackay, C.R. (2000). T-cell function and migration. Two sides of the same coin. N. Engl. J. Med. *343*, 1020–1034.

von Andrian, U.H., and Mempel, T.R. (2003). Homing and cellular traffic in lymph nodes. Nat. Rev. Immunol. *3*, 867–878.

von Herrath, M., and Whitton, J.L. (2001). Animal models using lymphocytic choriomeningitis virus. Curr. Protoc. Immunol. *Chapter 19*, Unit 19.10.

Weninger, W., Crowley, M.A., Manjunath, N., and von Andrian, U.H. (2001). Migratory properties of naive, effector, and memory CD8(+) T cells. J. Exp. Med. *194*, 953–966.

Wherry, E.J., Teichgräber, V., Becker, T.C., Masopust, D., Kaech, S.M., Antia, R., von Andrian, U.H., and Ahmed, R. (2003). Lineage relationship and protective immunity of memory CD8 T cell subsets. Nat. Immunol. *4*, 225–234.

Yoneyama, H., Matsuno, K., Zhang, Y., Nishiwaki, T., Kitabatake, M., Ueha, S., Narumi, S., Morikawa, S., Ezaki, T., Lu, B., et al. (2004). Evidence for recruitment of plasmacytoid dendritic cell precursors to inflamed lymph nodes through high endothelial venules. Int. Immunol. *16*, 915–928.